Springer

KSME

Journal of Mechanical Science and Technology 33 (1) (2019) 289~297
www.springerlink.com/content/1738-494x(Print)/1976-3824(Online)
DOI 10.1007/s12206-018-1228-z

Prescribed motion flow dynamics †

Md Zishan Akhter[1,2,*] and Ravi Chaithanya Mysa[3]

[1]*Department of Mechanical and Aerospace Engineering, Nanyang Technological University, Singapore*
[2]*Department of Aerospace Engineering, Technical University of Munich, Germany*
[3]*Department of Fluid Structure Interaction, Institute of High Performance Computing, A*STAR, Singapore*

(Manuscript Received May 25, 2018; Revised July 15, 2018; Accepted August 17, 2018)

Abstract

The numerical analysis of a circular cylinder undergoing oscillations in a two-dimensional laminar flow pattern, is performed in this paper. The cylinder is subjected to forced oscillations transverse to the free stream flow. A detailed analysis is presented for prescribed frequency ratios which are half, equal and double to that of the vortex shedding frequency. The prescribed motion amplitudes investigated range from 10-100 % of the cylinder diameter, at a fixed Reynolds number of 100. Detailed characteristics and field analysis of prescribed motion dynamics is presented in the paper. When the prescribed frequency matches shedding frequency, phase transition between transverse pressure force and displacement is witnessed along with the existence of a critical amplitude. The pressure distribution and evolution of wake contours with respect to the cylinder motion and excitation frequency is critically analysed to develop insight of the load development in the cylinder-fluid coupled system.

Keywords: Oscillating cylinder; Vortex shedding; Wake structure; Pressure; Lift

1. Introduction

The flow dynamics of an oscillating body in a flow has been a subject of interest among researchers for many years. The practical applications of this subject are primarily in the field of structural designing for marine bodies, off-shore exploration, and wind and power engineering. The coupling of motion and the flow-field gives rise to various physical phenomena such as vortex shedding and lock-on, hysteresis and bifurcation, etc. Better understanding of the force-dependence on transverse displacement is essential for designing robust cylindrical structures submerged in a fluid flow.

The earliest experiments on fluid-structure interaction were conducted in 1878 by Strouhal, on Aeolian tones. The problem of a cylinder oscillating in a crossflow or vice-versa representing wave-cylinder interaction has been investigated experimentally as well as numerically by many researchers around the world, majorly due to its significance in the field of ocean engineering. Some of the major contributions were done by Bishop and Hassan [1], Koopmann [2], Toebes [3], Griffin [4], Bearman and Currie [5], Bearman [6], Ongoren and Rockwell [7], Williamson and Roshko [8], Gu et al. [9], Meneghini and Bearman [10], Lu and Dalton [11], Blackburn and Henderson [12] and Guilmineau and Queutey [13].

*Corresponding author. Tel.: +91 8709040045
E-mail address: mdzishan001@e.ntu.edu.sg
† Recommended by Associate Editor Donghyun You

Bishop and Hassan [1] were the first to observe a jump in phase angle between the prescribed transverse force and the displacement of body. This phenomenon occurred when the excitation frequency was comparable to the shedding frequency of the body and was regarded as synchronisation condition. The change in phase angle was attributed to the alteration in the energy transfer across the cylinder-fluid system. Furthermore, the effect of forced oscillatory motion on vortex shedding pattern was studied in detail by Koopmann [2]. His studies were focussed on the determination of lock-in boundaries. He reported that a threshold oscillatory amplitude is needed to attain lock-in and its range is dependent on the motion amplitude. The flow dynamics and vortex shedding pattern around oscillating cylinder was studied by several researchers such as Toebes [3], Griffin [4] and Bearman [6]. Bearman and Curie [5] also investigated the pressure fields and fluctuations arising due to the coupling of fluid and oscillating cylinder. In study reported by Griffin and Ramberg [14], the Lock-on region was found to be about twice the Strouhal frequency. Zdravkovich [15] analysed the hike in phase angle between the displacement of body and vortex shedding at frequencies close to Strouhal frequency. He concluded that the exchange of energy in the fluid-body system is affected by phase change. Ongoren and Rockwell [7, 16] contributed greatly by validating the existing results as well as discovering the stable regions of vortex Lock-on. Apart from the Strouhal frequency, vortex shedding was demonstrated to be stable and

synchronized at half the Strouhal frequency. The effect of motion amplitude on the flow dynamics was studied in detail by Williamson and Roshko [8]. No difference was noted in the shedding pattern at low amplitudes while at higher values, the vortex street comprised of a vortex-pair on one side and a single vortex on the other. Gu et al. [9] performed experimental investigations into the flow dynamics of a cylinder undergoing oscillatory motion subjected to a range of excitation frequencies varying from 80 % to 120 % of the shedding frequency at Re = 185 and 5000. They observed vortex switching phenomenon occurring in the range of 112 % to 120 % of the shedding frequency. The experimental results of Gu et al. [9] were numerically reproduced at Re = 185 by Lu and Dalton [11] and Guilmineau and Queutey [13]. Blackburn and Henderson [12] studied the 2D flow dynamics of an oscillating cylinder in a cross flow. Hysteresis and bifurcation near Strouhal frequency as well as 2S to P + S vortex shedding transition, was validated by them. They concluded that the shift in phase and transition in shedding of vortices were due to the simultaneous acting of two separate vorticity generation mechanisms- oscillation and gradient of pressure around the body, respectively. A comprehensive review of the fluid structure interaction around a transversely oscillating cylinder has been published by Anagnostopoulos [17, 18]. Further, Sarpakaya et al. [19] studied the effects of the fluid-structure coupling on marine structures. Bearman et al. [20] studied the fluid forces acting around oscillating cylinder in a viscous flow, while Williamson [21] investigated sinusoidal flows. Obasaju et al. [22] studied fluid-structure interaction of a cylinder subjected to oscillating flow. The authors in Ref. [23] have studied in detail the variation of forces on transversely vibrating cylinder subjected to transverse flow. The computational complexities associated with the 3D flow-field around transversely oscillating cylinder has been addressed recently by Jiang et al. [24].

The previous studies reported in the literature discuss prescribed motion at low amplitudes and the lock-in of prescribed frequencies with the shedding frequency. Large variations of oscillatory amplitude at the shedding frequency needs to be studied to critically analyse the phase relation between forces and motion of the cylinder. Investigation of forces acting on the transversely moving cylinder and its effect on the phase relation it maintains with the displacement of the cylinder has not been studied in detail in the literature. The objective of this paper is to closely observe the fluid-structure interaction and the corresponding fluid dynamics generated due to the prescribed transverse motion of the cylinder for large domain of amplitude variation. Three different prescribed cylinder motion frequencies are considered for the study. First prescribed frequency is half of the shedding frequency, second one is equal to the shedding frequency and the third is twice of the shedding frequency. The interrelation between cylinder motion, flow dynamics and the generated forces, is critically analysed with respect to the phase relation. Based on the forces and flow contours, detailed explanation is provided for the phase behaviour variation with respect to amplitude of motion. This paper deals with the numerical analysis of a circular cylinder undergoing forced transverse oscillations in a laminar environment at Re = 100, over a wide range of forced-motion amplitude varying from (10 - 100) % of the cylinder diameter. The openFOAM based pimpleFoam is used for the numerical experiments.

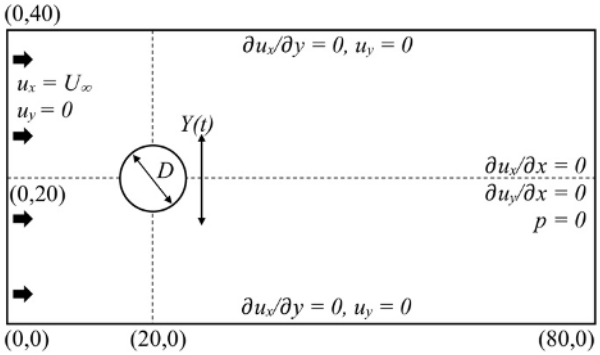

Fig. 1. Schematic diagram of computational domain and coordinate system along with boundary conditions.

The paper starts with introduction to the research topic and motivation for the work. It is followed by details of physical model and the numerical solver used in the study. The convergence tests and comparison studies are also included in this section. The next section is dedicated to the discussion and analysis of the obtained results. Eventually, the observations are concluded at the end of the paper.

2. Numerical methods

The cylinder is assumed to move in transverse direction to the fluid flow as shown in Fig. 1. The fluid force f(t) which is a function of time t is calculated from the numerical solution of the incompressible fluid flow. The governing equations for the incompressible fluid flow are:

$$\nabla.\mathbf{u} = 0 \tag{1}$$

$$\frac{\partial \boldsymbol{u}}{\partial t} + \nabla.\left(\left(\boldsymbol{u} - \boldsymbol{w}\right)\boldsymbol{u}\right) = -\frac{1}{\rho}\nabla \boldsymbol{p} + \nu\nabla^2\boldsymbol{u} \tag{2}$$

where $\boldsymbol{u}$ the flow velocity vector, $\boldsymbol{w}$ is the velocity of moving mesh and p is the scalar pressure, ρ is the density and v is the kinematic viscosity. The flow equations are solved only in x-y direction. PIMPLE algorithm in OpenFOAM is used to solve above equations on a deforming grid. The PIMPLE algorithm combines semi- implicit method for pressure-linked equations and pressure implicit splitting of operators. For solving pressure, geometric algebraic multi-grid solver is used and for solving velocity, preconditioned bi-conjugate gradient solver is used. The diagonal incomplete LU decomposition is used as preconditioner. The convergence criteria set for the solvers is 10^{-6}. The mesh motion equation which is a Laplacian equation of velocity is solved by preserving the mesh quality. The flow regime at Reynolds number of 100.

The computational domain schematic representing the incompressible two-dimensional flow on Cartesian axis is shown in Fig. 1. A structured domain of mesh size $0 \le x \le 80$ and $0 \le y \le 40$ is generated using GMSH software. A rigid cylinder of diameter D, is placed horizontally with its centre at (20, 20) on the Cartesian x-y domain. The longitudinal axis of the cylinder is aligned along the z-axis. A uniform crossflow of free stream velocity U_∞, enters the domain at x = 0 and flows in the positive x-direction. The domain boundaries on either side are symmetric.

The diameter of the cylinder D and free stream velocity U_∞, are used to non-dimensionalize variables. Likewise, Reynolds number is defined as $Re = U_\infty D/\nu$. The study is done at the fixed Reynolds number of Re = 100. The equation for the forced motion trajectory of the cylinder can be defined as:

$$Y(t) = A_e \sin(2\pi f_e t) \tag{3}$$

where Y(t) denotes the position of cylinder as a function of time as described in the works of Guilmineau and Queutey [13]. The amplitude ratio, A_r is obtained by the normalization of the oscillatory motion amplitude, A_e with the diameter of the rigid cylinder, D such that, $A_r = A_e/D$. The frequency ratio, $f_r = f_e/f_{St}$, where f_{St} is the Strouhal frequency. The simulations have been run for three frequency ratio cases of 0.5, 1.0 and 2.0. Further, the oscillatory motion amplitude ratio, A_r is varied from 0.1 to 1.0.

The force coefficients are characterized with respect to amplitude ratio and frequency ratio. The lift coefficient C_L and the drag coefficient C_D are:

$$C_L = \frac{1}{\frac{1}{2}\rho U^2 D}\int_S \left(p\hat{n} + \mu\left(\frac{\partial u_{\hat{t}}}{\partial \hat{n}} + \frac{\partial u_{\hat{n}}}{\partial \hat{t}}\right)\hat{t}\right)\cdot \hat{j} dS \tag{4}$$

$$C_D = \frac{1}{\frac{1}{2}\rho U^2 D}\int_S \left(p\hat{n} + \mu\left(\frac{\partial u_{\hat{t}}}{\partial \hat{n}} + \frac{\partial u_{\hat{n}}}{\partial \hat{t}}\right)\hat{t}\right)\cdot \hat{i} dS. \tag{5}$$

The unit vector $\hat{i}$ is in the direction of flow and $\hat{j}$ is in the transverse direction to the flow. The normal vector $\hat{n}$ and tangential vector $\hat{t}$ are with respect to the surface S, where $u_{\hat{t}}, u_{\hat{n}}$ are the velocities along the normal and tangent of the surface S. The density of the fluid is denoted by ρ and dynamic viscous coefficient is μ. The transverse lift force is important in oscillating cylinders where it varies non-linearly with the motion of the cylinder. The lift coefficient can further be decomposed into pressure and viscous components:

$$C_{Lp} = \frac{1}{\frac{1}{2}\rho^f U^2 D}\int_S (p\hat{n})\cdot \hat{j} dS \tag{6}$$

$$C_{L\mu} = \frac{1}{\frac{1}{2}\rho^f U^2 D}\int_S \left(\mu\left(\frac{\partial u_{\hat{t}}}{\partial \hat{n}} + \frac{\partial u_{\hat{n}}}{\partial \hat{t}}\right)\hat{t}\right)\cdot \hat{j} dS. \tag{7}$$

Table 1. Grid independence test for stationary case at Re = 100.

Mesh	Grid points	$C_{D,avg}$	$C_{L,rms}$
A	120000	1.3398	0.3177
B	150000	1.3393	0.3176
C	340000	1.3386	0.3174

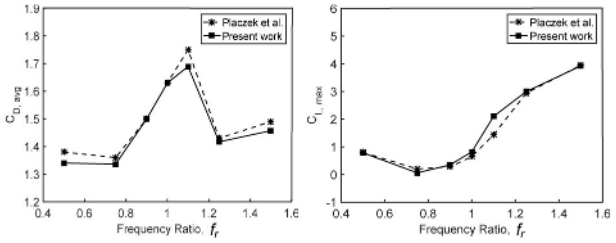

(a) (b)

Fig. 2. Aerodynamic coefficients for $A_r = 0.25$ over a range of f_r: (a) $C_{D,avg}$; (b) $C_{L,max}$.

Further, $C_{D,avg}$ denotes the time-averaged values of drag coefficient, while the root-mean squared values of lift coefficient are presented as $C_{L,rms}$.

2.1 Convergence and comparative studies

Grid independence was established by running the solution on grids of 120000 and 340000 grid points. The simulation results converged at 150000 with the convergence residual smaller than 10^{-3}, as shown in Table 1. The calculations for non-dimensional time-step were done using Courant-Friedrichs-Lewy condition of value CFL < 1.

The simulations were run for large time steps to ensure a statistically stable state for the computation of lift and drag coefficients. Various initial conditions were used to examine the effect of calculation time on the final stable flow-state achieved from the computation. In most of the cases, it was observed that the fully developed and stable/periodic state was attained upon reaching time step of $t \ge 100$. However, the computations were run for 1200 time units in all cases to ensure accuracy and minimal effect of calculation time on the ultimate flow-state.

The dependence of the temporal variations of aerodynamic coefficients upon excitation frequency and prescribed amplitude are consistent with Placzek et al. [25]. The lock-in zone exists between two symmetrical limits around the axis of f_r = 1.0 such that for $A_r = 0.25$ it ranges between $0.75 \le f_r \le 1.25$, according to the frontiers established by Koopmann [2]. A comparative study has been done at $A_r = 0.25$ for various frequency ratios such that the lock-in region is crossed. Maxima of $C_{D,avg}$ is attained within the lock-in zone at f_r = 1.1, as shown in Fig. 2(a). On the contrary, magnitude of $C_{L,max}$ is observed to drop initially before entering the lock-in zone, beyond which it shows continuous increment. However, amplification of lift force is less pronounced outside the lock-in region as can be seen in Fig. 2(b).

The comparative plots presented in Fig. 2 have similar trends globally with minor variation in the values obtained from Placzek et al. [25]. These differences can be traced back to the discrepancy in the values obtained for the fixed cylinder case where Placzek et al. [25] obtained the values of $C_{D,avg}$ and $C_{L,max}$ to be 1.37 and 0.33, respectively. While, in the present study these values are 1.339 and 0.317, respectively. Therefore, aspect ratio of the cylinder used in simulation could possibly result in variation in aerodynamic coefficients obtained.

3. Results and discussion

The oscillations in vortex-induced vibrations is known to be non-linear, where the forces vary complexly with respect to non-dimensional parameter reduced velocity [23, 26]. In the present set-up the cylinder motion frequency and amplitude are prescribed. The understanding of the force dependence on the prescribed motion parameters will help in linking the physics to the vortex-induced vibrations phenomenon. The frequency ratios considered for the numerical simulations are 0.5, 1.0 and 2.0, with amplitude ratio varying from 0.1 to 1.

3.1 Response characteristics

Fig. 3 shows the variation of lift coefficients with respect to amplitude ratio for frequency ratios of 0.5, 1.0 and 2.0. It should be noted that the values of $C_{L,rms}$ and $C_{LP,rms}$ corresponding to the f_r = 2.0 are scaled down by a factor of 2, to facilitate graphical observation. At lower frequency ratio of 0.5, as the amplitude ratio increases there is a gradual increase in the transverse load as shown in Fig. 3(a). At frequency ratio of unity, there is a non-linear variation in the transverse load with increase in amplitude ratio. There exists a critical amplitude ratio for f_r = 1.0, below which the transverse load decreases with increase in amplitude ratio. For amplitude ratio greater than 0.6, the transverse load increases with increase in amplitude ratio. The maximum amplitude for vortex-induced vibrations at Re = 100 in the lock-in region is near to 0.6 [23], which is the critical amplitude in the present prescribed motion dynamics. The flow physics for various amplitude ratios at the defined frequency ratios have to be critically analysed in order to understand the connection between the prescribed motion and vortex-induced vibrations. For frequency ratio of 2.0, there is increasing trend in transverse load with increase in amplitude ratio except for a dip at A_r = 0.8. For the cases of larger amplitude ratios A_r > 0.6, dependence of $C_{L,rms}$ on the magnitude of f_r becomes significant. Large transverse force is observed at frequency ratio of 2.0 compared to other two frequencies. The transverse force for A_r < 0.6, f_r = 1 is near to the values corresponding to f_r = 0.5.

The pressure and viscous contribution of $C_{LP,rms}$ and $C_{L\mu,rms}$ to the transverse force are plotted in Figs. 3(b) and (c), respectively. There is an increasing trend in viscous transverse force with respect to amplitude ratio. There is a non-linear trend in the pressure transverse variation with respect to amplitude ratio. The ratio $\left({}^{C_{L\mu,rms}}/_{C_{LP,rms}}\right)$ is plotted to in Fig. 3(d) to compare

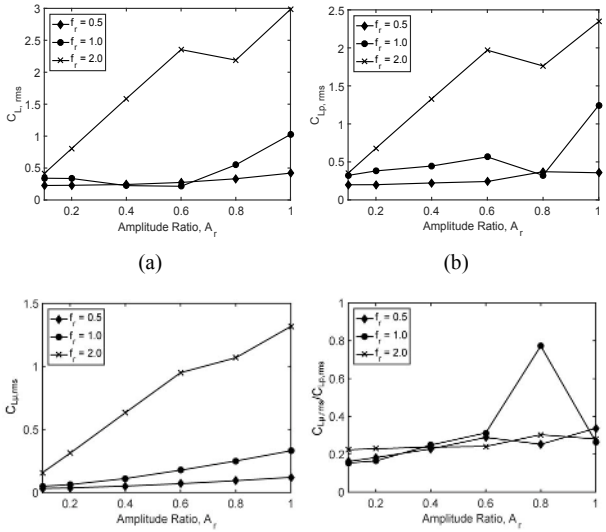

Fig. 3. Coupled response characteristics: Dependence of (a) $C_{L,rms}$; (b) $C_{LP,rms}$; (c) $C_{L\mu,rms}$ on A_r and f_r, at Re = 100; (d) ratio: $C_{L\mu,rms}/C_{Lp,rms}$.

the contribution of each to the transverse force. As the ratio is less than one, the pressure forces dominate over the viscous forces. For frequency ratio of 1, the ratio linearly increases upto critical amplitude of 0.6. The ratio suddenly increases at A_r = 0.8 and the value falls down after that. A critical examination of the phase difference between the forces and displacement of the cylinder and the vorticity contours is required to further investigate complex variation of transverse force with respect to amplitude ratio and frequency ratio.

3.2 Prescribed motion characteristics

The temporal response of transverse force and its phase relation with the prescribed motion is detailed in this section.

Fig. 4 shows the temporal variation of transverse force and its corresponding frequency content for amplitude ratio A_r = 0.1 to 1.0 and frequency ratio f_r = 0.5, 1.0 and 2.0. The frequency participation in the transverse force for different prescribed frequencies is plotted in the Fig. 5. Apart from the Strohaul frequency, there exists other frequencies in transverse force.

For f_r = 0.5, there exists three dominant frequencies for all the amplitude ratios considered. Upto A_r = 0.6, the primary frequency is the shedding frequency and secondary frequency is the prescribed frequency. For A_r > 0.6 the prescribed frequency becomes the primary frequency which shows the amplitude of motion has direct effect on the force amplitude. The third dominant frequency is thrice that of the prescribed frequency and remains the same throughout the range of oscillatory amplitudes considered. For f_r = 1.0, there exists two dominant frequencies in contrast to the previous case. Here, the prescribed and shedding frequencies are mapped together as the primary frequency, while the secondary frequency is thrice that of the shedding frequency. This phenomenon has

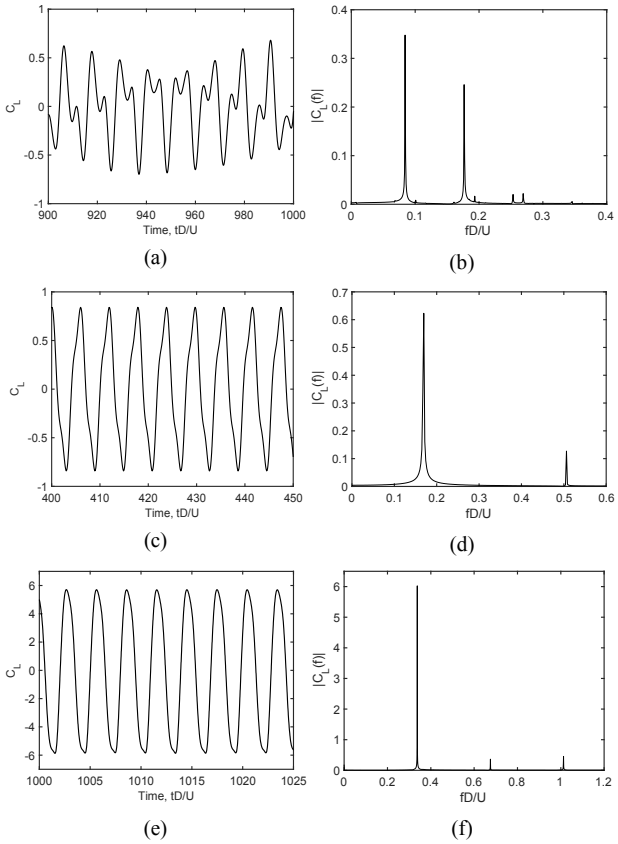

Fig. 4. Temporal variations of Lift coefficient (left) and frequency spectrum (right) at A_r =0.8, for: (a) and (b) f_r = 0.5; (c) and (d) f_r = 1; (e) and (f) f_r = 2.

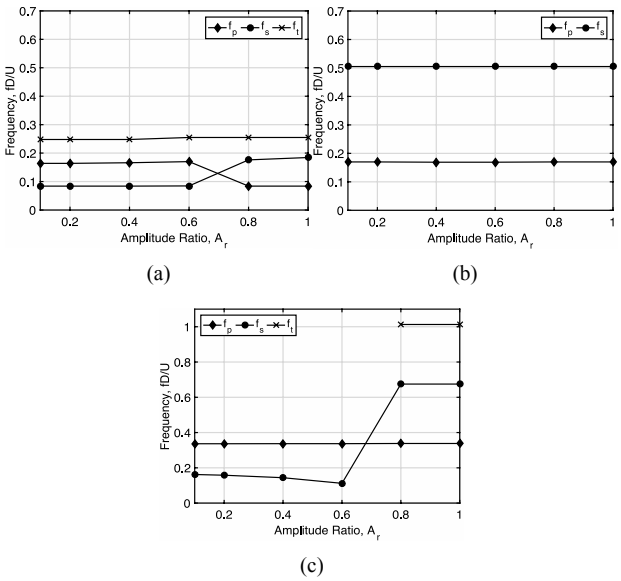

Fig. 5. Plots denoting frequency signals subject to 0.1 ≤ Ar ≤ 1.0 obtained for: (a) f_r = 0.5; (b) f_r = 1.0; (c) f_r = 2.0.

previously been observed by Ref. [23] with respect to vortex-induced vibrations in lock-in region. For f_r = 2.0 as shown in Fig. 5(c), the primary frequency content is always the prescribed frequency. The secondary frequency is the shedding frequency upto A_r = 0.6. Beyond A_r = 0.6, the secondary frequency is the one which is four times that of shedding frequency.

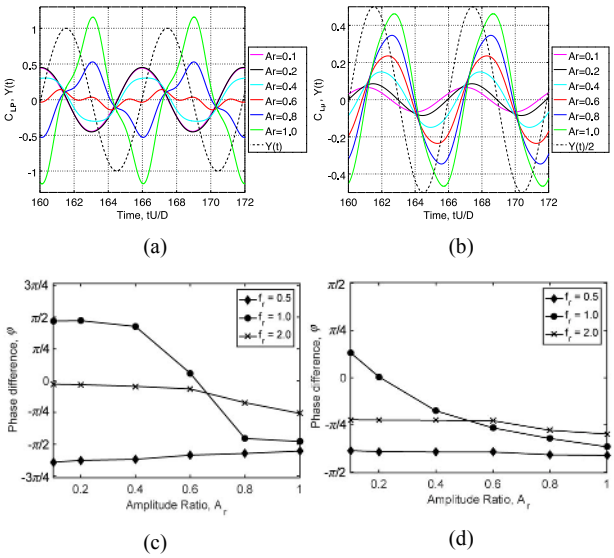

Fig. 6. Temporal variation of displacement Y(t): (a) C_{LP}; (b) $C_{L\mu}$, for f_r = 1.0. Phase difference between displacement Y(t): (c) C_{LP}; (d) $C_{L\mu}$.

To understand the load generation in cylinder-fluid coupled system, the phase relation between the transverse force and prescribed motion is plotted in Figs. 6(c) and (d). The temporal variation of transverse pressure forces and viscous forces along with cylinder displacement are plotted in Figs. 6(a) and (b), respectively for the case of f_r = 1.0. Transition in phase difference (φ) between coefficient of lift due to pressure, C_{LP} and displacement response, $Y(t)$ is evident in case of forced oscillatory motion of the cylinder. The transition occurs due to the transfer of energy to/from the cylinder-fluid system. The plot depicting difference in phase between C_{LP} and $Y(t)$, is shown in Fig. 6(c). A transition is noticed, when the cylinder is subjected to excitation frequency equal to that of the Strohaul frequency, i.e. f_r = 1.0. It is observed that for the amplitude ratio, $A_r \leq 0.4$, C_{LP} leads $Y(t)$ by π. The lift coefficient due to pressure is in phase with the cylinder velocity and therefore, energy is transferred to the system. While, for the case of A_r = 0.6, C_{LP} is almost in-phase with $Y(t)$ and lags velocity by a phase difference of π. Further, for $A_r \geq 0.8$, C_{LP} lags $Y(t)$ by a phase of π and is out of phase with the cylinder velocity. Eventually in these cases, the pressure forces dissipate energy and limit the coupled response of the system. The plot depicting difference in phase between $C_{L\mu}$ and $Y(t)$, is shown in Fig. 6(d). The lift coefficient due to viscosity is out of phase with the cylinder velocity. The phase differences between cylinder displacement $Y(t)$ and $C_{L\mu}$ for f_r = 0.5 and 2.0 are nearly constant at -π/3 and -π/4, respectively. The phase transition is observed in case of f_r = 1.0, such that the phase difference between $C_{L\mu}$ and Y(t) decreases continuously with the increment in A_r. Thus, it can be concluded that the viscous forces

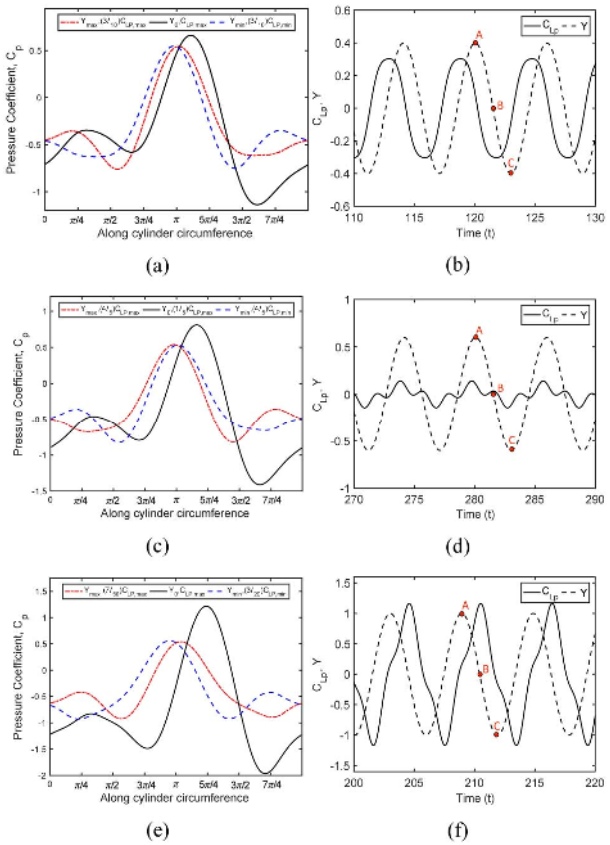

Fig. 7. (a), (c), (e) Distribution of C_P over the cylinder circumference at Y_{max}, Y_{zero} and Y_{min} displacements; (b), (d), (f) temporal variation of C_{LP} and Y(t) with points A, B and C highlighting Y_{max}, Y_{zero} and Y_{min} positions of the cylinder, respectively. The cylinder is subjected to f_r = 1.0: (a) and (b) A_r = 0.4; (c) and (d) A_r = 0.6; (e) and (f) A_r = 1.0.

extract energy from the cylinder-fluid system and limits the overall coupled response.

Progressively, the effects of vortex-body interactions on the pressure distribution around cylinder and the analysis of resultant wake contours, over the predefined range of force amplitudes and excitation frequencies is performed in the upcoming section.

3.3 Pressure distribution and wake contours

Pressure coefficient provides insight of the fluid forces acting around the cylinder. The phase difference between the transverse pressure force and displacement of the cylinder is almost constant for f_r = 0.5. However, for the cases of f_r = 1.0 and 2.0, the phase difference is not constant and varies with amplitude ratio. Therefore, a detailed discussion of the pressure and corresponding wake contours are done.

The pressure distribution on the cylinder for f_r = 1 and A_r = 0.4, 0.6 and 1.0 are shown in Figs. 7(a), (c) and (e), respectively, whereas the corresponding temporal variation of transverse load due to pressure and the displacement of the cylinder are plotted in Figs. 7(b), (d) and (f), respectively. The pressure contours are plotted at specific instants of *Ymax*, *Yzero* and *Ymin* which are marked as points A, B and C in the temporal variation of displacement Y(t). At A_r = 0.4, the transverse force due to pressure C_{LP} leads the displacement by $\pi/2$ as shown in Fig. 7(b), whereas C_{LP} lags the displacement by $\pi/2$ as seen in Fig. 7(f). The transition of phase difference between the transverse force due to pressure and motion of the cylinder from $\pi/2$ to $-\pi/2$ is approximately around A_r = 0.6, which is represented as the critical amplitude. The critical amplitude A_r may represent the maximum amplitude of the cylinder in the lock-in region of the vortex induced vibrations. Also, the maximum amplitude of cylinder in the lock-in region is 0.6, with a phase difference of zero value [23]. The stagnation pressure as well as the suction pressure increases with the increase in amplitude of motion A_r and they are maximum at mean position where the velocity is maximum. The contribution of force in the transverse direction due to the stagnation pressure is opposite in direction to the contribution of suction pressure. For $A_r < 0.6$, the transverse force due to suction pressure dominates over the stagnation pressure where by the transverse force leads the motion of the cylinder. As the transverse force due to pressure is in phase with the cylinder velocity, there is a supply of energy from the fluid forces due to pressure, to sustain the motion of the cylinder. As the amplitude of motion A_r increases the stagnation point shifts farther away from the $\theta = \pi$ towards the larger suction pressure side as shown in pressure distribution of Figs. 7(a), (c), (e) and the vorticity contours Figs. 8(b), 8(e) and 8(h). For $A_r > 0.6$, the stagnation pressure contribution to the transverse direction dominates over the contribution from the suction pressure which leads to transverse pressure force to lag behind the motion of the cylinder by $\pi/2$. This is majorly due to the shifting of stagnation pressure more towards the larger suction pressure side. The transverse pressure force is out of phase with the velocity of the cylinder and acts against the motion of the cylinder for $A_r > 0.6$. Thus, this motion of the cylinder above the critical amplitude is not sustained as the forces due to pressure act against the motion of the cylinder. From this it is clear that the maximum displacement of a cylinder in vortex-induced vibration cannot be larger than the critical amplitude of the prescribed motion cylinder because the motion is not sustained as the fluid forces acts against it.

The vorticity contours for f_r = 1, A_r = 0.4 at positions *Ymax*, *Yzero* and *Ymin* are shown in Figs. 8(a)-(c), respectively. At maximum displacement of the cylinder the clockwise vortex has been already formed on the upper region of the cylinder. As the cylinder moves from the maximum position towards the mean position, the vortex on the lower region of the cylinder starts rolling and is fully formed as the cylinder moves to the minimum position. A similar trend is found for the amplitudes A_r = 0.6 and 1.0 as shown in Figs. 8(d)-(i). The vorticity is spread larger in transverse direction with increase in amplitude of motion.

At f_r = 2.0 the phase difference between the transverse force due to pressure and the displacement of the cylinder is ap-

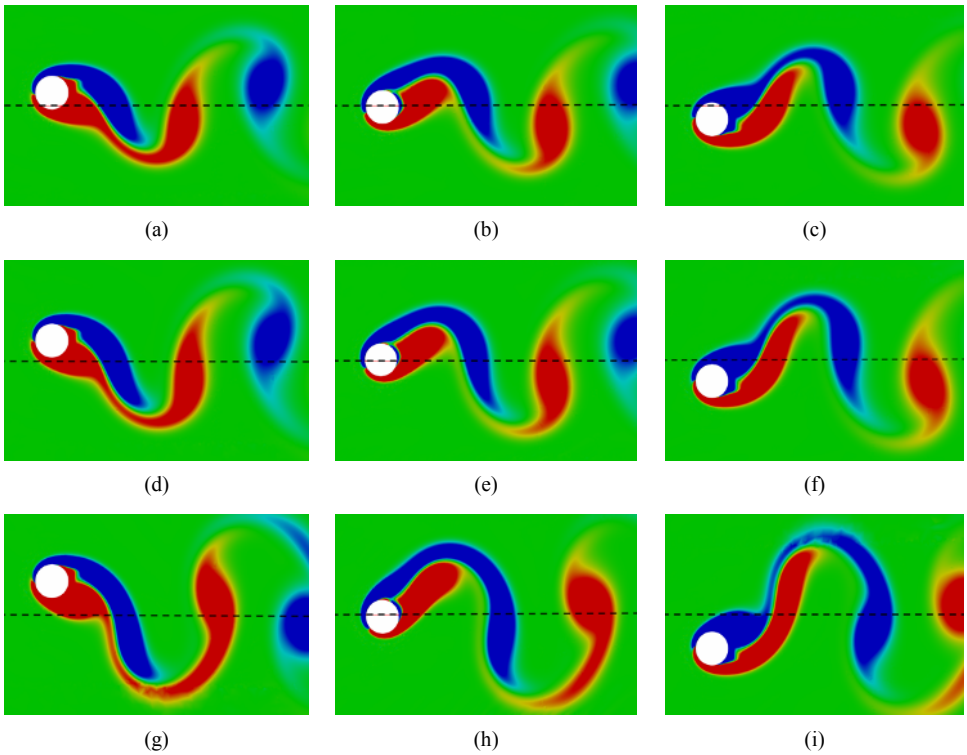

Fig. 8. Plots showing wake contours at cylinder positions of Y_{max} (Left), Y_{zero} (Centre) and Y_{min} (Right); subjected to (a)-(c) f_r = 1.0 and A_r = 0.4; (d)-(f) f_r = 1.0 and A_r = 0.6; (g)-(i) f_r= 1.0 and A_r =1.0.

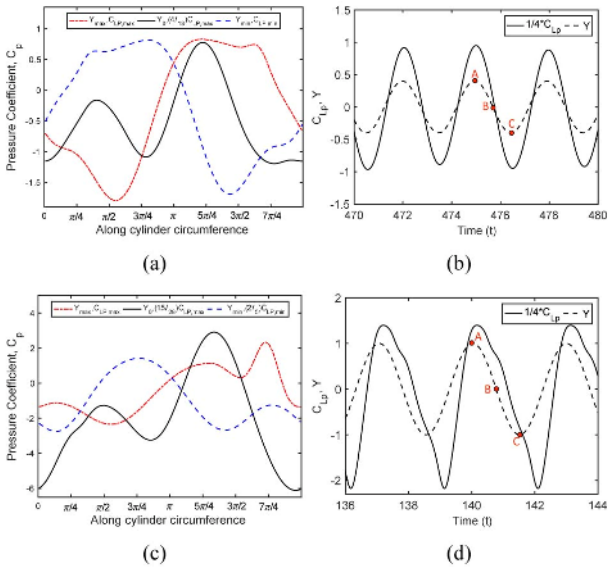

Fig. 9. (a), (c) Distribution of C_P over the cylinder circumference at Y_{max}, Y_{zero} and Y_{min} displacements; (b), (d) temporal variation of C_{LP} and Y(t) with points A, B and C highlighting Y_{max}, Y_{zero} and Y_{min} positions of the cylinder, respectively. The cylinder is subjected to f_r = 2.0: (a) and (b) A_r = 0.4; (c) and (d) A_r = 1.0.

proximately zero for lower amplitudes of motion $A_r \leq 0.6$. The phase difference decreases with increase in amplitude and reaches $-\pi/4$ at $A_r = 1.0$. Two representative cases of $A_r = 0.4$ and 1.0 are chosen for further analysis to represent phase differences of $\varphi = 0$ and $-\pi/4$, respectively. The temporal variation of the transverse pressure force and displacement at A_r = 0.4, are shown in Fig. 9(b), where both the signals are in-phase. At point A, large suction pressure is found on the upper region of the cylinder. Due to separation on the lower region of the cylinder as shown in Fig. 10(a), the pressure on the lower region is almost equivalent to the stagnation pressure which leads to very large transverse load. At point C, the separation is on the upper region of the cylinder, where the cylinder is at minimum position. Increase in the forced motion amplitude results in phase transition such that displacement *Y(t)* lags behind the transverse force due to pressure *(C_{LP})*, as can be observed from Figs. 9(c) and (d) for the case of A_r = 1.0. At A_r = 0.4, 2S vortices are shed as seen through the Figs. 10(a)-(c). Further, Figs. 10(d)-(f) show the vorticity contours for the cylinder at A_r = 1.0, where the vortex shedding pattern is characterised by 1P+1S. This leads to the change in phase difference between transverse pressure force and transverse motion of the cylinder from approximately zero at A_r = 0.4 to $-\pi/4$ at A_r = 1.0. Asymmetry in the vortex shedding is observed for $A_r \geq 0.6$ and leads to 1P+1S for $A_r \geq 0.8$ as shown in Fig. 11. The clockwise vortex strength in 1P vortex is comparatively lesser than the anti-clockwise one. The clockwise vortex strength in 1P shedding is minimal in case of A_r = 0.8, and gradually becomes stronger as witnessed in case of A_r = 1.0. This asymmetric shedding is the reason for the phase difference deviation. The vortex switching phenomenon with increment in forced amplitude from typical 2S to 1P+1S in case of f_r = 2.0, can be attributed to a pair of vortex generat-

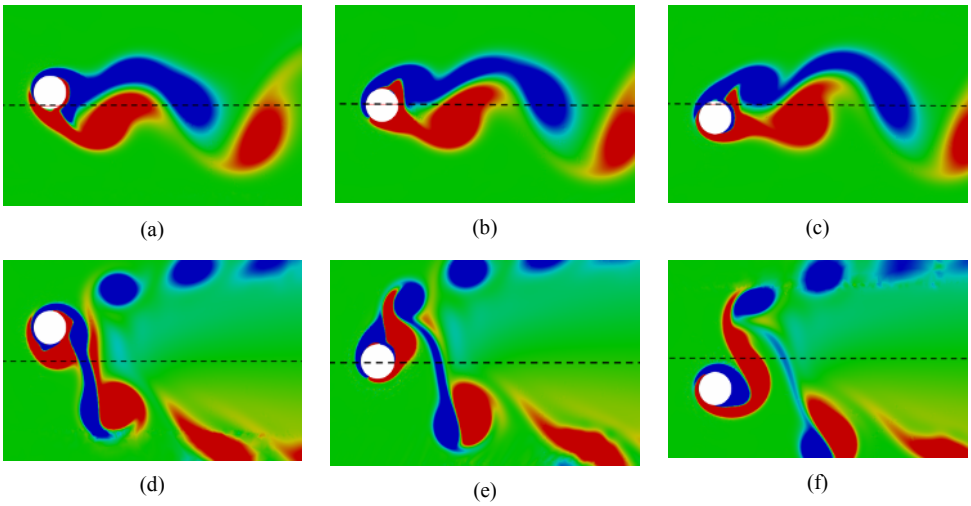

Fig. 10. Plots showing wake contours at cylinder positions of Y_{max} (Left), Y_{zero} (Centre) and Y_{min} (Right); subjected to (a)-(c) $f_r = 2.0$ and $A_r = 0.4$; (d)-(f) $f_r = 2.0$ and $A_r = 1.0$.

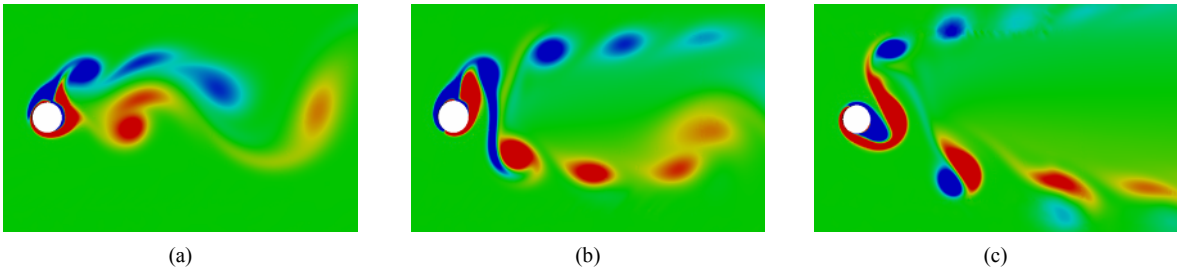

Fig. 11. Vortex switching phenomenon as observed in the wake contours of $f_r = 2.0$ subjected to: (a) $A_r = 0.6$; (b) $A_r = 0.8$; (c) $A_r = 1.0$.

ing mechanisms which are oscillatory motion and the pressure gradient, acting simultaneously upon the cylinder-fluid system [12]. Effect of the excitation frequency on the flow dynamics and vorticity is in agreement with the experimental results. It was demonstrated by Ongoren and Rockwell [7] and Gu et al. [9], that with the decrease in the excitation frequency, the vorticity in the wake region appear to be more spaced along the longitudinal direction and vice-versa, as can be compared in Figs. 8 and 10.

4. Conclusions

In this paper, numerical investigation of the prescribed motion flow dynamics of a circular cylinder in a two-dimensional laminar flow is done. The computations were done for three excitation frequencies having six different oscillatory amplitudes. The simulations were run for $Re = 100$, $0.1 \leq A_r \leq 1.0$ and $f_r = 0.5$, 1.0 and 2.0.

The temporal variation of lift coefficient showed dependence on the excitation frequency as well as the oscillatory amplitude. The root-mean-squared values of lift coefficient $C_{L,\mathrm{rms}}$ increases with f_r for low amplitude ratios, having sharp rise in cases of $f_r = 2.0$. The behaviour of $C_{L,rms}$ in cases of $f_r = 0.5$ and oscillatory amplitudes of $0.2 < A_r \leq 1.0$ was non-linear, such that a minima was attained at $A_r = 0.6$. The plots for C_{LP} and $C_{L\mu}$ showed the same pattern as of the primary C_L curve, with the magnitude of C_{LP} being greater than $C_{L\mu}$ in all the cases.

Load response generated for the case of $f_r = 0.5$ recorded a transition in primary frequency from f_{St} to f_e, as the oscillatory amplitude increased beyond 60 % of the cylinder diameter. Likewise, a transition in the secondary frequency between $0.6 < A_r \leq 0.8$ was noticed for the case of $f_r = 2.0$. Tertiary frequency signals were also traced in this case for $A_r \geq 0.8, f_r = 2.0$.

Phase difference between C_{LP} and displacement response $Y(t)$ was mapped to investigate the load generation in the system. A transition in the phase from $\pi/2$ to $-\pi/2$ was noticed in case of $f_r = 1.0$ as the oscillatory amplitude increased beyond 60 % of cylinder diameter. This amplitude is regarded as the critical amplitude A_r of the cylinder. This critical amplitude is equal to the maximum amplitude in the lock-in region of vortex-induced vibrations.

For $f_r = 1.0$ and $A_r \leq 0.6$, the transverse force due to suction pressure dominated over the stagnation pressure. The shift in stagnation point with the increment in A_r towards the larger suction pressure side i.e. $\theta > \pi$, was visualised in the respective wake contours. As the amplitude ratio A_r increased beyond 0.6, the shift in stagnation pressure as well as increase in its magnitude resulted in phase transition such that transverse pressure force lagged behind the cylinder motion by $\pi/2$. Thus, the transverse pressure force acted against the motion of the cylinder. For $f_r = 2.0$ and $A_r \leq 0.6$, the transverse force due to pressure and the displacement of the cylinder are in-phase.

However, further increment in the motion amplitude resulted in the reduction of phase difference, attributed to the switching of wake structure from 2S to 1P+1S for $A_r \geq 0.8$.

References

[1] R. E. D. Bishop and A. Y. Hassan, The lift and drag forces on a circular cylinder oscillating in a flowing fluid, *Proc. of the Royal Society,* London, UK (1964) A277 51-75, Doi: 10.1098/rspa.1964.0005.

[2] G. H. Koopmann, The vortex wakes of vibrating cylinders at low reynolds numbers, *Journal of Fluid Mechanics*, 28 (1967) 501-512, Doi: 10.1017/s0022112067002253.

[3] G. H. Toebes, The unsteady flow and wake near an oscillating cylinder, *Journal of Basic Engineering*, 91 (1969) 493-505, Doi: 10.1115/1.3571165.

[4] O. M. Griffin, The unsteady wake of an oscillating cylinder at low reynolds number, *Journal of Applied Mechanics*, 38 (1971) 729-738, Doi: 10.1115/1.3408948.

[5] P. W. Bearman and I. G. Currie, Pressure-fluctuation measurements on an oscillating circular cylinder, *Journal of Fluid Mechanics*, 91 (1979) 661-677, Doi: 10.1017/s002211 2079000392.

[6] P. W. Bearman, Vortex shedding from oscillating bluff bodies, *Annual Reviews of Fluid Mechanics*, 16 (1984) 195-222, Doi: 10.1146/annurev.fluid.16.1.195.

[7] A. Ongoren and D. Rockwell, Flow structure from oscillating cylinder part 1. mechanisms of phase shift and recovery in the near wake, *Journal of Fluid Mechanics*, 191 (1988) 197-223, Doi: 10.1017/s0022112088001569.

[8] C. H. K. Williamson and A. Roshko, Vortex formation in the wake of an oscillating cylinder, *Journal of Fluids and Structure*, 2 (1988) 355-381, Doi: 10.1016/s0889-9746(88)90058-8.

[9] W. Gu, C. Chyu and D. Rockwell, Timing of vortex formation from an oscillating cylinder, *Physics of Fluids*, 6 (1994) 3677-3682, Doi: 10.1063/1.868424.

[10] J. R. Meneghini and P. W. Bearman, Numerical simulation of high amplitude oscillatory flow about a circular cylinder, *Journal of Fluids and Structure*, 9 (1995) 435-455, Doi: 10.1006/jfls.1995.1025.

[11] X.-Y. Lu and C. Dalton, Calculation of the timing of vortex formation from an oscillating cylinder, *Journal of Fluids and Structure*, 10 (1996) 527-541, Doi: 10.1006/jfls.1996.0035.

[12] H. M. Blackburn and R. D. Henderson, A study of two-dimensional flow past an oscillating cylinder, *Journal of Fluid Mechanics*, 385 (1999) 255-286, Doi: 10.1017/ s0022112099004309.

[13] E. Guilmineau and P. Queutey, A numerical simulation of vortex shedding from an oscillating circular cylinder, *Journal of Fluids and Structure*, 16 (2002) 773-794, Doi: 10.1006/jfls.2002.0449.

[14] O. M. Griffin and S. E. Ramberg, Vortex shedding from a circular cylinder vibrating inline with an incident uniform flow, *Journal of Fluid Mechanics*, 75 (1976) 257-276, Doi: 10.1017/s0022112076000207.

[15] M. M. Zdravkovich, Modification of vortex shedding in the synchronization range, *Journal of Fluids Engineering*, 104 (1982) 513-517, Doi: 10.1115/1.3241895.

[16] A. Ongoren and D. Rockwell, Flow structure from an oscillating cylinder, part 2 model competition in the near wake, *Journal of Fluid Mechanics*, 191 (1988) 225-245, Doi: 10.1017/s0022112088001570.

[17] P. Anagnostopoulos, Numerical study of the flow past a cylinder excited transversely to the incident stream, part 1: Lock-in zoned, hydrodynamic forces and wake geometry, *Journal of Fluids and Structure*, 14 (2000) 819-851, Doi: 10.1006/jfls.2000.0302.

[18] P. Anagnostopoulos, Numerical study of the flow past a cylinder excited transversely to the incident stream, part 2: Timing of vortex shedding, aperiodic phenomena and wake parameters, *Journal of Fluids and Structure*, 14 (2000) 853-882, Doi: 10.1006/jfls.2000.0303.

[19] T. Sarpkaya, M. Isaacson and J. V. Wehausen, Mechanics of wave forces on offshore structures, *Journal of Applied Mechanics*, 49 (1982) 466, Doi: 10.1115/1.3162189.

[20] Bearman et al., Forces on cylinders in viscous oscillatory flow at low keulegan-carpenter numbers, *Journal of Fluid Mechanics*, 154 (1985) 337-356, Doi: 10.1017/s002211 2085001562.

[21] C. H. K. Williamson, Sinusoidal flow relative to circular cylinders, *Journal of Fluid Mechanics*, 155 (1985) 141-174, Doi: 10.1017/s0022112085001756.

[22] E. D. Obasaju, P. W. Bearman and J. M. R. Graham, A study of forces, circulation and vortex patterns around a circular cylinder in oscillating flow, *Journal of Fluid Mechanics*, 196 (1988) 467-494, Doi:10.1017/s0022112088002782.

[23] R. C. Mysa, A. Kaboudian and R. K. Jaiman, On the origin of wake-induced vibration in two tandem circular cylinders at low Reynolds number, *Journal of Fluids and Structures*, 61 (2016) 76-98.

[24] Jiang et al., Flow around an oscillating cylinder: computational issues, *Fluid Dynamics Research*, 49 (2017) 055505 (14pp).

[25] A. Placzek, J. Sigrist and A. Hamdouni, Numerical simulation of an oscillating cylinder in a cross-flow at low reynolds number: Forced and free oscillations, *Computers and Fluids*, 38 (2009) 80-100, Doi: 10.1016/j.compfluid.2008.01.007.

[26] J. S. Leontini, M. C. Thompson and K. Hourigan, The beginning of branching behaviour of vortex-induced vibration during two-dimensional flow, *Journal of Fluids and Structures*, 73 (2006) 857-864.

Md Zishan Akhter is currently pursuing Masters in Aerospace Engineering, jointly from Nanyang Technological University (Singapore) and Technical University of Munich (Germany). He specializes in Aerodynamics and Propulsion with keen interests in Space Propulsion.